SHEAR DEFORMATION OF RADIATION RECRYSTALLIZED NEAR SURFACE FACETS

David J. Walters*, Edward E. Adams, Patrick J. Staron, Ladean R. McKittrick
Montana State University, Bozeman, Montana

ABSTRACT: A layer of radiation recrystallized near surface facets was produced in a controlled environmental chamber at Montana State University. Environmental conditions prescribed to produce the weak layer were obtained from field observations. This layer is tested using a GeoTac - GeoJac load actuator attached to a steel shear frame similar to the standard field test. A GOM - ARAMIS optical analysis device is used to record strain at 15 measurements per second. ARAMIS captures high resolution, three dimensional deformation data for a vertical profile of stratified snow containing the developed weak layer. Deformation data is graphically superimposed over real-time photos of the profile. An area showing maximum strain corresponding to the bounds of the weak layer prior to fracture propagation is apparent. Microscopic images at the location of the rupture within the weak layer identify the presence of facets on one or both sides of the fracture plane. Using the deformation data, the magnitude and direction of the strain field is calculated across the exposed surface profile. The strain field in the weak layer orients into an organized pattern of tension and compression consistent with the direction of shearing. In comparison, cohesive slab snow above and below the weak layer show little straining (randomly oriented strain vectors are artifacts of strain too small to calculate), indicating near rigid body displacement. These observations provide a clearer understanding of weak layer deformation immediately prior to fracture.

KEYWORDS: Radiation Recrystallization, Shear, Strain, Optical, Mechanics, Snow

1. INTRODUCTION

A method to ascertain strain fields in a controlled laboratory environment is presented. Recognizing that dry slab avalanches typically initiate on weak layers (Bader and Salm, 1990; Fukuzawa and Narita, 1992; Jamieson and Schweizer, 2000; McClung, 1987; Schweizer, 1998; Schweizer, 1999; Schweizer et al., 2003), this study has been undertaken to better understand dry slab avalanche initiation at weak layers in the snow pack. Two techniques for testing snow in shear include displacement controlled shear testing (de Monmollin, 1982; Fukuzawa and Narita, 1992; Joshi et al., 2006; McClung, 1977) and load controlled shear testing (Podolskiy et al., 2008; Reiweger et al., 2010). The use of displacement controlled testing was chosen in this study due to its simplicity of setup.

* *Corresponding Author Address:*
David J. Walters, Civil Engineering,
Montana State University, 205 Cobleigh Hall,
Bozeman, MT 59717-3900; tel: 406-994-6104;
Email: david.walters@ce.montana.edu

Radiation recrystallized faceted layers were developed in the laboratory using a protocol similar to that established by Morstad (2004) and Slaughter et al. (2009; 2008). Environmental conditions were chosen based on the parameters determined in Slaughter et al. (2009). These faceted layers were then tested in situ using displacement rate-controlled tests to examine the strain field leading to failure.

Displacement and strain on each sample was analyzed using an optical strain measuring system. This device is conceptually similar to the Particle Image Velocimetry (PIV) used by Gleason (2006) and more recently, Reiweger et al. (2010), however, it achieves a faster capture rate (up to 15 frames per second).

Initial testing with a tilting, displacement rate controlled shear testing actuator and optical strain measurements shows promise in analyzing displacement and deformation in and around weak regions in the snow.

2. LABORATORY AND EQUIPMENT

A fully programmable environmental cold chamber was used for the development and testing of the mechanical properties of radiation recrystallized snow layers. Parameters include incoming shortwave radiation, incoming longwave radiation, air temperature, humidity and airflow across a sample. Solar simulation is provided by a metal-halide luminary. Longwave radiation is provided through a temperature controlled ceiling. Imposed environmental parameters for this study were chosen based on the results of Slaughter et al. (2009). Thermocouple arrays with 1 cm vertical spacing are inserted in the top 10 cm of the snow to measure snow temperature with depth.

Loading of the snow sample is controlled using a GeoTac – GeoJac load actuator developed for soils testing that was adapted for use in this study. The actuator can be displacement-rate or load-rate controlled up to a maximum displacement of 5.08 cm and load of 2.2 kN. The actuator is mounted to a rigid frame capable of orienting the load at any angle between horizontal (0°) and vertical (90°) (Figure 1). The onboard data-logger records both actuator displacement and load at a rate of 1Hz maximum. This data is collected on a system separate from the sample strain and displacement data.

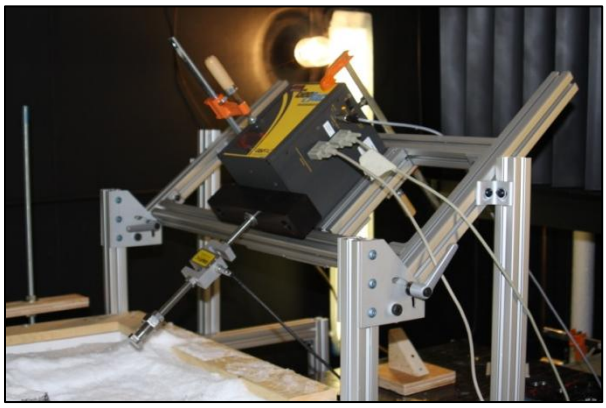

Figure 1: Loading frame mechanism with GeoTac - GeoJac actuator attached

The shear frame used during all of the experiments is one typically found in many field study kits; 16 cm square, 4 cm tall. It is constructed from 1.5 mm thick stainless steel with two internal fins (thus creating three separate open regions). Instead of pulling on the frame, as is typical in field methods, the actuator is configured to push on the frame.

Strain and displacement data (including principal strain magnitudes and directions, maximum shear strain among others) is obtained using a GOM-Aramis optical strain measuring device (Figure 2). Displacement is the measure of how far a point has moved from its original position. Strain is a dimensionless parameter that measures the change in position of a point relative to a neighboring point. Axial strain (ε) is measured in percent ($\varepsilon = \delta l / l_o \times 100$). The device uses two cameras to obtain a stereological 3-D mapping of the surface being measured. The supporting software uses image recognition algorithms to track a speckle pattern applied onto the test specimen. Using the first image as reference, the software tracks changes in the pattern to calculate deformation down to 2-3 microns for simple materials and 10-15 microns for snow (determined from calibration data stored with each experimental setup). If the two cameras are in disagreement over “seeing” the same spot on the sample, a “hole” in the overlaid analytical layer is produced. This can happen with porous materials since one camera may be able to see into the pore while the other cannot. Erroneous strain measurements can develop around the holes.

Figure 2: GOM-Aramis system

3. EXPERIMENTAL PROCEDURES

Three tests with similar setups were investigated. Snow samples were placed in a 70 x 70 x 50 cm box with an open top and insulated vertical walls. The snow was harvested during the late winter of 2010 and stored for later testing. The snow was removed from storage as needed in order to replace the top 10-20 cm of snow in the experimental box that was discarded after each test. The experimental setups including initial crystal type, initial density, incoming shortwave radiation, incoming longwave radiation, ambient air temperature, average surface temperature and maximum temperature gradient are summarized in Table 1. All experiments had zero surface wind.

After the recrystallization process was stopped, the snow was covered for 10 minutes to allow temperature gradients to subside. Next, a new layer of snow was sieved 5 to 10 mm thick. This created a surface for the shear frame to rest above the newly formed faceted crystals. This placement was used to avoid inducing a stress concentration within the presumed weak layer. Figure 3 shows the placement of the shear frame within the snow sample. After placing the shear frame on the new surface 5-10 mm above the faceted layer, snow was sieved in and around the shear frame to completely cover it. The snow was allowed to sinter around the frame for several hours, permitting the snow added following recrystallization to form an upper slab layer, with the shear frame securely embedded in it.

The snow profile tested contains a base slab layer, a thin layer of radiation recrystallized facets, and a top slab layer containing the shear frame (Figure 3). It is important to note that the faceted layer was recrystallized within the top of the bottom slab layer. In order to isolate the column of snow under the shear frame, snow was carefully cut away on all four sides down to the bottom boundary of the faceted layer. The column was kept short to minimize bending imparted on the column. The side of the profile facing the Aramis cameras was cut further down to include the base slab with the other layers for strain and displacement analysis.

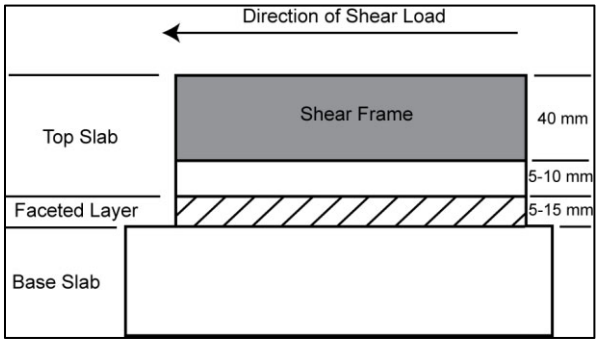

Figure 3: Snow profile showing layering of slabs and faceted layers. The shear frame is placed so that it is 5-10 mm above the faceted layer. The column is cutout only to the bottom depth of the faceted layer

The exposed surface facing the Aramis cameras is marked with a fine dot pattern of black paint for the Aramis image recognition software. The angle of the load actuator is adjustable to allow combined loading. In a horizontal configuration (direct shear), the actuator and inline load cell are placed to push the frame from right to left relative to all figures shown. After calibration, the camera system is positioned to analyze the profile of the column of snow.

Table 1: Summary of radiation recrystallization environmental conditions for the duration of the experiment. Radiation values and temperature values remained near constant for the duration of the experiment

	Initial Crystal Type	Initial Density (kg/m^3)	Incoming Shortwave (W/m^2)	Incoming Longwave (W/m^2)	Ambient Air Temperature (°C)	Mean Surface Temp (°C)	Max Temp Gradient (°C/m)	Recrystal-lization. Duration (hrs)
T1	Decomposing stellar dendrites, small Rounds	175	630-635	230	-10	-6.5	350	50
T2	Small Rounds	144	640-650	245	-10	-6.8	180	20
T3	Decomposing stellar dendrites, small rounds	96	600-605	245	-10	-5.5	210	23

4. PRELIMINARY RESULTS

Three tests on snow containing radiation recrystallized facets were completed. Two of the tests were conducted under direct shear loading conditions (no externally supplied vertical force). A third was conducted with the load being applied at 50 degrees from vertical (see Figure 8). Load versus *actuator displacement* was recorded separately from the Aramis snow displacement and strain data. Microscope images of crystals before the shear test help verify the thickness of the faceted layer, and images taken after the shear test help identify the location of fracture within the layers of snow.

4.1 Test 1 (T1): Direct shear in snow containing a layer of radiation recrystallized facets

Using the conditions listed in Table 1, T1 formed a layer of radiation recrystallized facets about 5 mm thick (see Figure 4) The sample was loaded horizontally from right to left (relative to all figures shown) at a rate of 0.0423 mm/s for just over 184 seconds to failure.

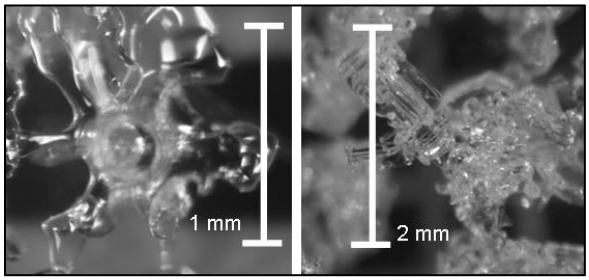

Figure 4: (Left) before recrystallization; (Right) after recrystallization. Faceted crystals found about 5 mm thick

The load actuator reached a maximum load of 143 N with actuator displacement at 7.8 mm just prior to fracture. In comparison, Aramis data indicated that the top slab underwent a nearly uniform maximum leftward displacement of 0.02 mm at 67 ms (the last image) before fracture (Figure 5). The two maximum displacements could have been reported at slightly different times during the test since the actuator and Aramis could not be started simultaneously. Local deformation of the frame (visible bow in loaded frame surface) accounted for the difference in recorded displacements.

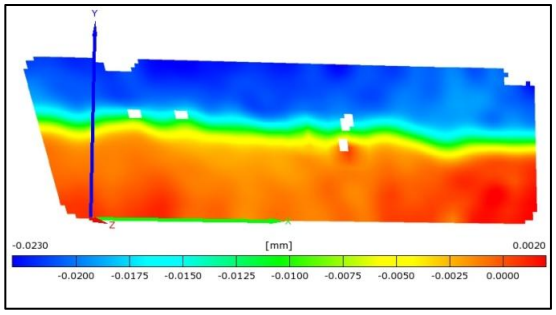

Figure 5: Horizontal displacement 67 ms before fracture of the snow in T1 while loaded from right to left. Note the area of steepest gradient is consistent with the location of the weak layer. The top edge of the displacement data is also the bottom edge of the shear frame. The bottom slab remained stationary and rigid while the top slab had constant displacement indicative of rigid body displacement. (See Section 2 regarding white holes in image)

Along with displacement, maximum strain magnitude and direction intensify to around 0.200-0.240 % in tension just before fracture. The area of most intense straining occurred in the faceted layer. Optical microscope images of the crystals above and below the fracture plane confirm that the fracture occurred within the faceted layer. Notice that at two frames (130 ms) before fracture in Figure 6.a, disorganized strain vectors indicate no measurable strain is detected, but one frame (67 ms) before fracture in Figure 6.b strain directions organize along the area experiencing the maximum principal strain. The nearly 45° orientation of the strain field along the weak layer is consistent with the expectations of snow loaded in direct shear. Compressive principal strains were oriented perpendicular to and about half the magnitude of the tensile principal strains.

4.2 Test 2 (T2): Direct shear in snow containing a layer of radiation recrystallized facets

T2 formed a 15 mm thick layer of radiation recrystallized facets above a melt freeze layer using conditions listed in Table 1. It is interesting to note that a melt-freeze layer developed presumably due to the only slightly lower snow density and higher radiation input relative to T1. The column of snow under the frame was cut down to the beginning of the melt freeze layer (see Figure 3). T2 was also loaded in direct shear from right to left (relative to the figures) at a rate of 0.0423 mm/s.

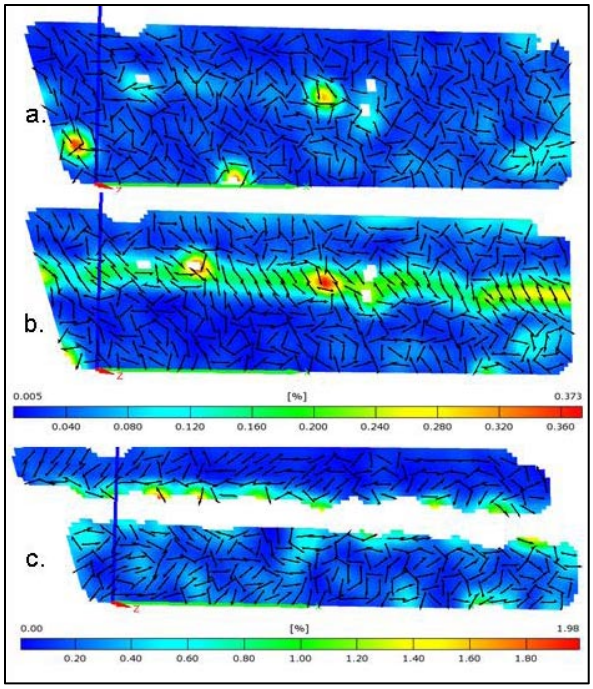

Figure 6: a) Maximum principal strain of T1 133 ms before fracture; b) 67 ms before fracture; c)Fracture in T1 (color is magnitude in % strain; vectors indicate maximum strain directions). Note that fracture occurred along the same area experiencing the most straining prior to fracture.

T2 produced a maximum actuator load of about 43.5 N at an actuator displacement of 0.7 mm prior to fracture.

T2 displayed measurable strain starting about 8 seconds before fracture/collapse. Due to larger pore spaces in the faceted layer of T2 than previous tests (known from visual inspection), the following images contain noisier data (see Section 2 about Aramis image calculation). The following sequence of images in Figure 7 show a time lapse of T2 during loading with maximum strain magnitudes superimposed over the real-time images. At 6.67 seconds (Figure 7a) elapsed time, there was no measurable strain. At 13.33 seconds (Figure 7b), measurable strain began in the faceted layer. Strain magnitudes continued to increase up to fracture. Strain intensified rapidly to around 0.75 % in the final second before fracture at 21.93 seconds (Figure 7e). Maximum principal strain directions in the faceted layer also developed near 45° tensile orientations with

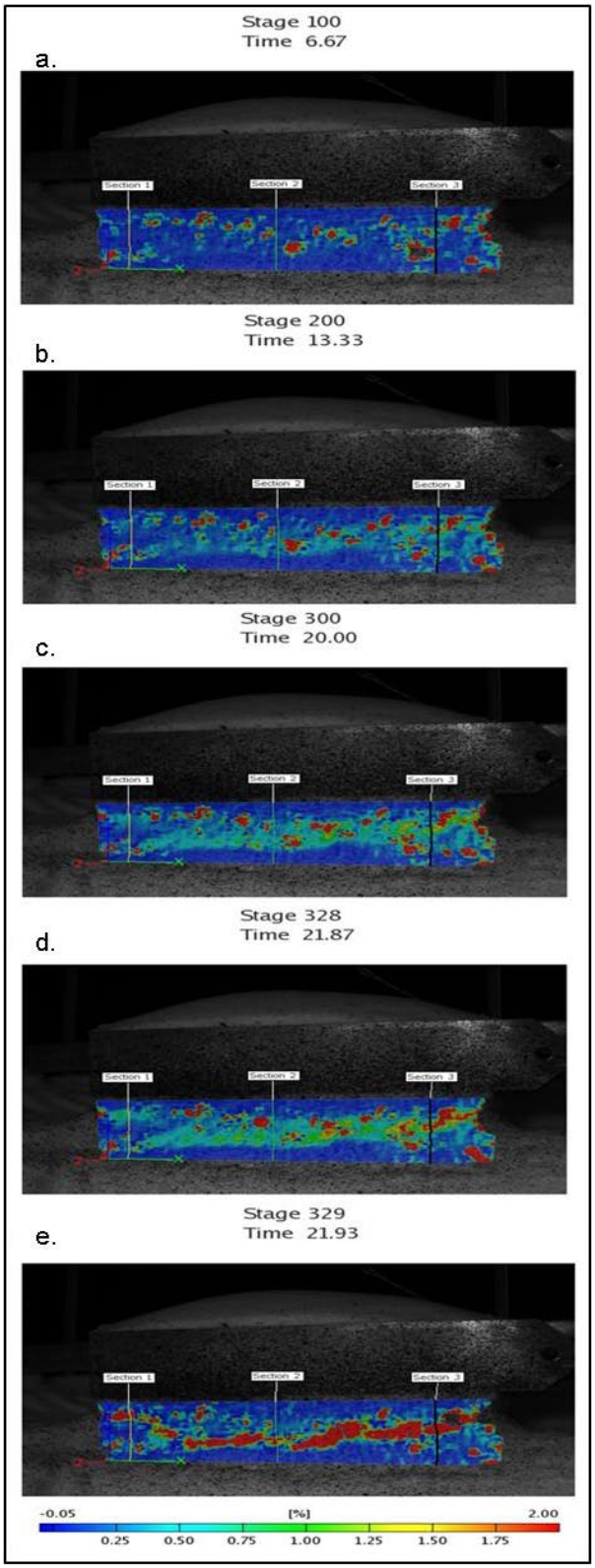

Figure 7: Image sequence of maximum strain % during shear loading on T2. Initial signs of straining occur in 7.b and continue until failure. Fracture occurred at 7.e

compressive principal strain perpendicular to and to nearly half the magnitude of the tensile principal strain recorded in T1 in Figure 6.b.

The bed surface of the fracture followed the highlighted region of Figure 7e very closely. Microscope images of crystals taken from the top of the fracture plane showed good evidence of faceted crystals, whereas crystal images from the bed surface of the fracture showed no faceting present. This evidence indicates that the fractured layer in T2 failed at the bottom of the faceted layer and above the melt-freeze interface. The melt-freeze layer provided the sliding surface after fracture

4.3 Test 3 (T3): Simultaneous vertical and shear loading in snow containing a layer of radiation recrystallized facets

Unlike the previous 2 tests, T3 formed 1-3 mm needle like facets 5-7.5 mm thick using the parameters listed in Table 1. Warmer surface temperatures may have contributed to this development although were not significantly warmer than previous tests (see Table 1). These needle-like facets are consistent with radiation recrystallized facets observed during field studies at the Yellowstone Club during the winter of 2008 (McCabe et al., 2008; Slaughter et al., 2009; Slaughter et al., 2008). T3 was loaded at 50° from vertical (equivalent to 50° slope) as seen in Figure 8. The displacement rate along the angle was increased to 0.106 mm/s to achieve the same shear displacement rate (horizontal displacement rate) as the previous two tests.

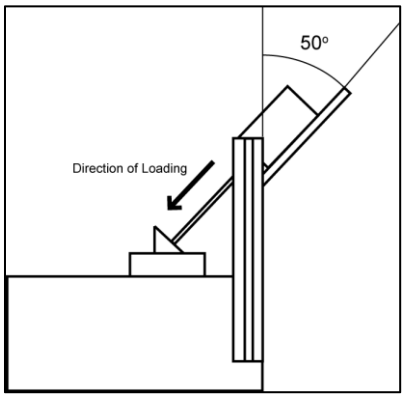

Figure 8: Schematic of loading scheme used during T3

T3 produced a maximum actuator load of 138 N (shear component of 105.7 N and a normal component of 88.7 N). The faceted layer appeared, from the images, to fail under shear and collapse modes due to the more complex loading conditions, but the sequence of the modes could not be determined.

A measurable strain field developed about 10 seconds before fracture and intensified rapidly in the final 500 ms before fracture. Figure 9 shows the sequence of maximum principal strain developing during the loading of the sample. Strain develops slowly at elapsed times of 6.67 s and 13.33 s (Figure 9a and Figure 9b respectively). Maximum principal strain intensifies to 1–1.75 % 70 ms before rupture (Figure 9c). Finally rupture occurs in the region bounded by highest strain (Figure 9d). Inspection of microscope images revealed faceted crystals above and below the fracture plane indicating fracture in the middle of the layer.

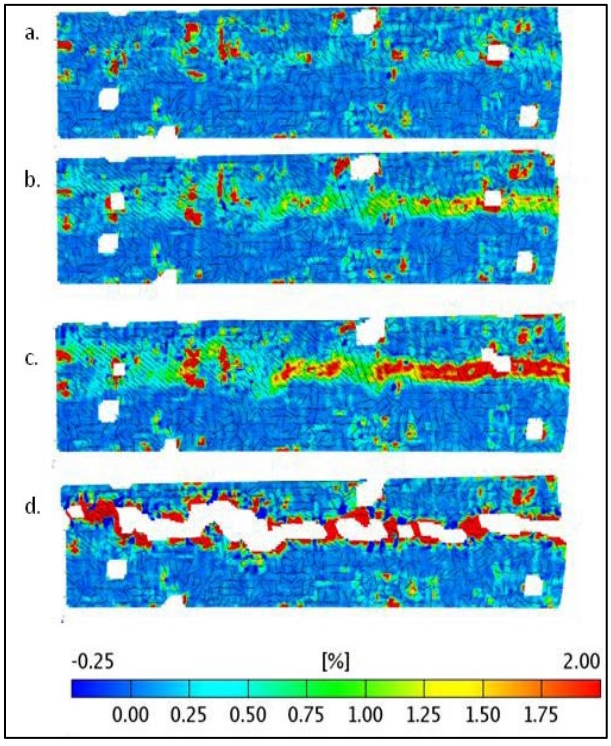

Figure 9: Sequence of major strain developing during loading: a. 6.67 s elapsed; b. 13.33 s elapsed; c. 16.60 s elapsed; d. Fracture 16.67 s elapsed

5. DISCUSSION

All three tests showed strong evidence of three distinct layers in the snow containing different strength properties. Comparing Figure 6, Figure 7, and Figure 9, the top and bottom slab layers show no strain occurring while the layer in between, which contained radiation recrystallized faceted crystals, showed significant straining. The area with most straining also highlighted the region where fracture occurred. This verifies that the faceted crystals that were developed are the weakest layer in these samples. Microscope images of the crystals found around the fracture plane confirm that the failure occurred in the faceted layer.

Since the area undergoing the most straining in the image is coincident with the bounds of the region containing faceted crystals, a faceted layer thickness can also be obtained from the strain images. Figure 10a and b. show a comparison of ε_{xy} (tensor shear strain, ½ engineering shear strain) in T1 and T2 respectively 67 ms before fracture. The area undergoing most straining in Figure 10a is only half as thick as the similar are in Figure 10b. Aramis data indicate the faceted weak layer in T1 was about 5–7 mm thick and the similar layer in T2 was 10–15 mm thick. These depths were confirmed with microscope images of crystals taken from different depths.

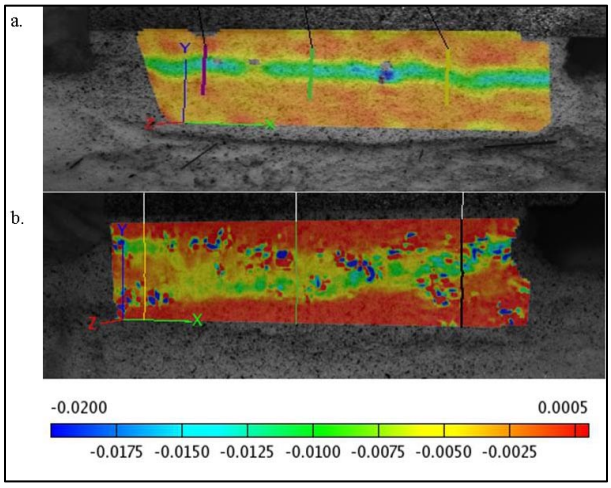

Figure 10: ε_{xy} (shear strain) 67 ms before fracture in T1 (a.) and T2 (b.). Notice that the layer with highest magnitude of shear strain in a. is only half as thick as the higher magnitude of shear strain in b.

Also, all of the strain images of T1 show maximum straining took place in a fairly smooth, linear region — as was the fracture plane — indicating a shear quality 1 (Johnson and Birkeland, 2002). The strain images of T2 and T3 show a less linear region of peak straining with several small humps and ridges. Likewise, the resulting fracture in both T2 and T3 followed these areas of straining resulting in a fracture of shear quality 2 in each test. Shear quality 2 implies a mostly smooth fracture surface with minor irregularities (Johnson and Birkeland, 2002).

6. CONCLUSIONS AND FUTURE WORK

Development of techniques to measure strain optically in snow during loading shows great promise. The tests above show the ability to examine deformation on a small scale at relatively high frame capture rates. The data produced shows that strain and deformation concentrates inside the bounds of the faceted layers present in the snow sample. Using optical microscope images of crystals found on either side of the fracture plane verify that fracture occurs somewhere between the faceted layer boundaries. This indicates that faceted layers in snow are weak layers.

Further analysis of current and future experiments aim to compare the experimentally derived quantities of stress and strain against current material models used for snow. Reliable directional strength data is critical for further development and understanding of avalanche initiation in models and in the field.

7. ACKNOWLEDGEMENTS

We are grateful to the U.S. National Science Foundation (grants # 0521360, 0635977, 0922765) and the Murdock Charitable Trust. The work was conducted at the Montana State University Subzero Science and Engineering Facility.

8. REFERENCES

Bader, H.P. and Salm, B., 1990. On the mechanics of snow slab release. Cold Regions Science and Technology, 17(3): 287-300.

de Monmollin, V., 1982. Shear tests on snow explained by fast metamorphism. Journal of Glaciology, 28(98): 187-198.

Fukuzawa, T. and Narita, H., 1992. An experimental study on the mechanical behavior of a depth hoar layer under shear stress, International Snow Science Workshop, Breckenridge, Colorado, USA, pp. 171-175.

Gleason, A., 2006. Particle image velocimetry: A new technique to measure strain in loaded snow. The Avalanche Review, 24(3): 12.

Jamieson, B. and Schweizer, J., 2000. Texture and strength changes of buried surface-hoar layers with implications for dry snow-slab avalanche release. Journal of Glaciology, 46(152): 151-160.

Johnson, R.F. and Birkeland, K.W., 2002. Integrating shear quality into stability test results, International Snow Science Workshop, Penticton, British Columbia, CANADA.

Joshi, S., Mahajan, P. and Upadhyay, A., 2006. Study of layered snow under shear and tension, International Snow Science Workshop, Telluride, Colorado, USA, pp. 165-173.

McCabe, D., Munter, H., Catherine, D., Henninger, I., Cooperstein, M., Leonard, T., Adams, E.E., Slaughter, A.E. and Staron, P.J., 2008. Near-Surface Faceting on South Aspects in Southwest Montana, International Snow Science Workshop, Whistler, British Columbia, CANADA, pp. 147-154.

McClung, D., 1977. Direct simple shear tests on snow and their relation to slab avalanche formation. Journal of Glaciology, 19(81): 101-109.

McClung, D.M., 1987. Mechanics of snow slab failure from a geotechnical perspective, Avalanche Formation, Movement, and Effects, Davos Symposium. IAHS, Davos, SWITZERLAND, pp. 475-508.

Morstad, B.W., 2004. Analytical and Experimental Study of Radiation-Recrystallized Near-Surface Facets in Snow, Montana State University, Bozeman, Montana, USA, 204 pp.

Podolskiy, E., Chernous, P., Abe, O., Barashev, N. and Nishimura, K., 2008. Experimental study of short-term loading influence on shear strength, International Snow Science Workshop, Whistler, British Columbia, CANADA, pp. 701-708.

Reiweger, I., Schweizer, J., Ernst, R. and Dual, J., 2010. Cold Regions Science and Technology Load-controlled test apparatus for snow. Cold Regions Science and Technology, 62(2-3): 119-125.

Schweizer, J., 1998. Laboratory experiments on shear failure of snow. Annals of Glaciology, 26: 97-102.

Schweizer, J., 1999. Review of dry snow slab avalanche release. Cold Regions Science and Technology, 30(1-3): 43-57.

Schweizer, J., Jamieson, J.B. and Schneebeli, M., 2003. Snow Avalanche Formation. Reviews of Geophysics, 41(4).

Slaughter, A.E., McCabe, D., Munter, H., Staron, P.J., Adams, E.E., Catherine, D., Henninger, I., Cooperstein, M. and Leonard, T., 2009. An investigation of radiation-recrystallization coupling laboratory and field studies. Cold Regions Science and Technology, 59(2-3): 126-132.

Slaughter, A.E., Staron, P.J., Adams, E.E., McCabe, D., Munter, H., Catherine, D., Henninger, I., Cooperstein, M. and Leonard, T., 2008. Laboratory simulations of radiation-recrystallization events in southwest montana, International Snow Science Workshop, Whistler, British Columbia, CANADA, pp. 139-146.